NJC

ROYAL SOCIETY OF CHEMISTRY

PAPER

View Article Online
View Journal | View Issue

Cite this: *New J. Chem.*, 2024, **48**, 13917

Coal fly ash derived zeolite: a solid-state base for convenient synthesis of diphenyl ethers†

Aashima Mahajan,[a] Manmohan Chhibber*[a] and Loveleen K. Brar *[b]

Received 17th April 2024,
Accepted 11th July 2024

DOI: 10.1039/d4nj01781a

rsc.li/njc

Worldwide, the ever-rising demand for coal in power plants has increased coal fly ash (CFA) production. Its disposal is a major environmental problem. CFA zeolitization offers a possible alternative for converting this hazardous solid waste into high-value products. This work uses the fusion-assisted ultrasonication method to synthesize zeolite. The material was characterized using X-ray diffraction (XRD), field emission scanning electron microscopy (FE-SEM), energy-dispersive X-ray spectroscopy (EDS), Fourier transform infrared (FTIR) spectroscopy, Brunauer–Emmett–Teller (BET) and Barrett–Joyner–Halenda (BJH) techniques. The synthesized zeolite, sodalite was mesoporous with a surface area of 22.13 m^2 g^{-1} and an average pore size of 7 nm. This was used and optimized as a solid-state base for synthesizing diphenyl ethers (DPEs). The yields of twelve diphenyl ethers with aldehyde, chloro, methoxy, methyl and nitro groups ranged from 35 to 91%. The methodology offers an advantage over conventional processes in providing single-step synthesis of DPEs with electron-withdrawing groups on both rings.

1. Introduction

Rapid industrialization and population growth have led to a substantial rise in energy demand. The dominance of coal-fired thermal power plants in the energy sector has resulted in massive production of coal fly ash worldwide.[1,2] Recent energy demands predict that fly ash production will rise to 300–400 million tons in the future.[3] This industrial waste has resulted in multiple problems like shortage of storage space, land contamination resulting in damage to plant and animal life, and many health problems like asthma, lung cancer, respiratory problems, premature death, and chronic bronchitis.[4–6] It is essential to find ways to mitigate this problem. Recently, fly ash has found applications in the cement industry, construction of roads, and building materials.[7,8] About 20% of fly ash is being used constructively, but a significant amount is still disposed of in open pits.[9] There exists a broad scope for exploring derivatives of this product by making new materials for potential applications in water purification, agriculture, organic reactions, petrochemistry, and many others.[10–12]

The composition of fly ash suggests the presence of quartz and mullite, along with ferrous and other impurities.[13,14] Zeolites are three-dimensional crystalline microporous materials made by different arrangements of aluminosilicates and have pores with sizes ranging from 1 to 10 Å.[15] These materials have diverse applications in gas sensing, environmental remediation, catalytic activity, and the pharmaceutical industry. Thus, ample opportunity exists to modify fly ash into zeolites and explore different applications. These can be synthesized from coal fly ash using fusion-assisted hydrothermal or conventional heating methods but require long reaction times and high temperatures.[9,11] Recently, microwave- and ultrasound-assisted methods have been employed to reduce the time and temperature of zeolite synthesis.[16,17]

The surface of zeolites has diverse groups that allow interactions with different organic substrates for use in organic reactions like transesterification, coupling reactions, Knoevenagel reactions, isomerization, oxidation, carbonylation, and many others.[18–24] Surface functionalization of zeolites is important in carrying out specific organic reactions. For example, surface methoxy groups on mordenite were key intermediates for methane-to-methanol conversion.[25] Similarly, the Kaolin-based zeolite surface was functionalized with amine groups to sequester CO_2 from the air.[26] Manique *et al.* used active sites present in sodalite as a catalyst for the transesterification reaction of soybean oil.[27] Further, Valdes *et al.* explored the use of the surface hydroxyl groups present in natural zeolite for catalytic ozonation of water-contaminated methylene blue dye.[28]

Recently copper-I-exchanged zeolites were shown to catalyze Ullman-type synthesis of diphenyl ethers (DPEs).[29] DPEs have diverse applications. For example, triclosan and its derivatives are used as antibacterial agents in hygiene products, and polybrominated diphenyl ethers are used as flame retarding

[a] *Department of Chemistry and Biochemistry (DCBC), Thapar Institute of Engineering and Technology, Patiala 147004, Punjab, India. E-mail: mchhibber@thapar.edu*
[b] *Department of Physics and Material Science (DPMS), Thapar Institute of Engineering and Technology, Patiala, 147004 Punjab, India. E-mail: brarloveleen@thapar.edu*

† Electronic supplementary information (ESI) available. See DOI: https://doi.org/10.1039/d4nj01781a

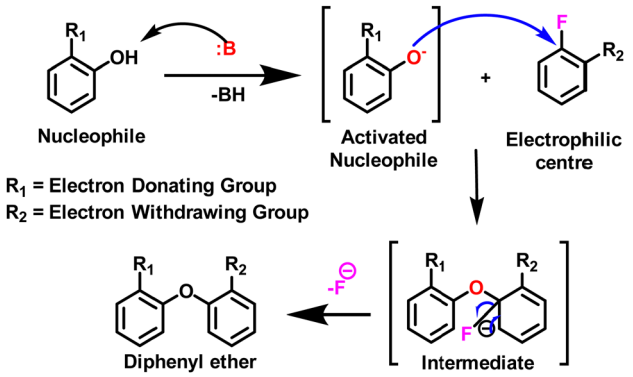

Scheme 1 Conventional diphenyl ether (DPE) synthesis using traditional bases (:B) like K_2CO_3, $CsCO_3$, *etc.*

materials.[30,31] Violacerol-I, isolated from marine resources, is an antifungal agent.[30–32] Considering the biological and material importance of DPEs, it was envisioned to use fly-ash-modified zeolites for DPE synthesis.

This work presents the conversion and characterization of industrial coal fly ash into sodalite using ultrasonication. The material was used as a solid-state base for synthesizing diphenyl ethers. Solid-state bases have an advantage over conventional ones (K_2CO_3, Cs_2CO_3, NaOH, *etc.*) due to their ease of separation, non-corrosive nature, and convenient disposal. DPE synthesis, in general, requires a reaction between an electron-rich phenol and an electron-deficient aromatic halide (Scheme 1). It further requires multi-step manipulation of the functional groups to have electron-withdrawing groups on both rings. Commercially available zeolites and the use of microwaves have also been reported to give single-step DPEs with electron-withdrawing groups on both rings.[33,34] To our knowledge, coal fly ash-derived sodalite has never been used to synthesize DPE and with electron-withdrawing groups on both rings. Therefore, the present methodology of DPE synthesis offers an advantage over the traditional ones.

DPE synthesis with different substrates was carried out after optimizing synthetic conditions like the reaction time and temperature, solvent, and mole percent of the sodalite. Diphenyl ether derivatives containing functional groups like nitro, methoxy, aldehyde, methyl, and chlorine were synthesized in 35–91% yields.

2. Materials and methods

2.1 Materials

Coal fly ash (CFA) was a gift from Guru Gobind Singh Super Thermal Power Plant, Ropar (Punjab), India. Sodium hydroxide (Loba Chemie, 97%) and sodium aluminate (Otto Chemika-Biochemika) were commercially purchased and used without further purification. All washing and dilution processes were done using distilled water (Organo Biotech Laboratories Pvt. Ltd). A centrifuge (Thermo Fisher Scientific, 8000 rpm) was used to collect suspended materials from the dispersions, and an ultrasonic probe (ChromTech, 100W/220V/5A) was used for the aging process.

Fig. 1 Schematic representation of the synthesis of sodalite from coal fly ash.

2.2 Pretreatment of fly ash

CFA was passed through a 200 mesh sieve, washed multiple times to remove water-soluble impurities, and dried in an oven at 80 °C. After washing, the fly ash (1 g) was mixed with water (100 mL) and stirred for 30 minutes. The resulting suspension was kept still for 5 minutes, so denser particles settled down due to gravity. The supernatant was decanted and centrifuged. The separated smaller particles (**S-CFA**) were dried at 100 °C. **S-CFA** was heat-treated at 800 °C (5 °C min^{-1}) for two hours to get rid of volatiles. The heat-treated **S-CFA** was further soaked in 10% HCl and washed with water until the neutral pH to remove metallic impurities.[9,16] Finally, it was dried in a hot-air oven and designated as **FA**.

2.3 Synthesis of sodalite

Zeolite was synthesized using the fusion-assisted ultrasonic method with slight modifications as shown in Fig. 1. **FA** and NaOH in a ratio of 1 : 1.4 and sodium aluminate (to balance Si : Al = 1 : 1) were ground using a pestle and mortar, transferred to a nickel crucible, and fused in a muffle furnace at 750 °C for 2 h. After cooling to room temperature, the fused material was again ground and dispersed in water (1 g/10 mL) using an ultrasonic probe (3 h). The obtained homogeneous gel was crystallized by heating in an oil bath at 110 °C for 16 h. The crystalline material was collected, washed with distilled water to neutral pH, and dried overnight in an oven at 80 °C. It was then characterized using XRD, FESEM, BET, and FTIR. Section S1 (ESI†) gives details of the optimization steps for the fusion process.

2.4 Characterization techniques

To investigate the phase composition of the prepared zeolites, X-ray diffraction line profile data (XRD, SmartLab SE Rigaku (Cu Kα radiation, 1.54 Å)) within the range of 5°–80° and a step size of 0.013° were analyzed. The morphology and elemental analyses of the initial and synthesized materials were performed using a field-effect scanning electron microscope (FE-SEM; Carl-Zeiss Sigma 500 FEG-SEM at an operating voltage of 20 kV) and an energy dispersive X-ray spectrometer (EDX Bruker, QUANTAX 200). Fourier-transform infrared spectroscopy (FTIR Shimadzu IRTracer-100 from 400 cm^{-1} to 4000 cm^{-1}) was used to analyze the functional groups in fly ash and synthesized zeolite. The

surface area and pore diameter were calculated using Brunauer–Emmett–Teller (BET) and Barrett–Joyner–Halenda (BJH) methods using adsorption–desorption isotherms of nitrogen (Micromeritics ASAP 2020). The thermal behaviour of the synthesized zeolite was investigated using thermogravimetric analysis (NETZSCH-STA 449 F3 Jupiter) in the presence of air from room temperature to 800 °C at a heating rate of 5 °C min^{-1}.

The point of zero charge pH_{pzc} represents a specific pH at which the charge on the sample surface is zero. pH_{pzc} for the synthesized zeolite was determined using the salt addition method. NaOH and HCl were used to adjust the pH of 5 mM NaCl solutions (10 mL) from 3 to 12. Each solution consisting of 3 mg of the synthesized zeolite was stirred for 24 h, and the change (ΔpH) from the initial pH (pH_i) was measured. A graph was plotted between the change in pH (ΔpH along the *Y*-axis) and the initial pH (along the *X*-axis) to calculate the value of point of zero charge (pH_{pzc}).

2.5 Synthesis of DPE

Aryl halides, phenols, and solvents used to synthesize diphenyl ether derivatives were procured from Spectrochem, Avra, Sigma-Aldrich, and Loba Chemie. The progress of the reaction was monitored using thin layer chromatography (TLC; Silica gel 60 F_{254}, Analytical Chromatography), and the yield was calculated using nuclear magnetic resonance (NMR) 400 MHz (JEOL) spectroscopy having $CDCl_3$ as the solvent. Details of NMR data analysis for yield determination and calculations for individual products are given in sections S2 and S3 (ESI†), respectively. High-resolution mass spectrometry (HRMS) was performed on a Waters XEVO-G2XSQTOF spectrometer to confirm the mass of the synthesized derivative.

2.6 General method for the synthesis of diphenyl ethers (DPEs) using zeolite

1-Fluoro-2-nitrobenzene (1 equivalent) and the corresponding phenol/8-hydroxyquinoline (1 equivalent) were dissolved in DMSO (6 mL) using a 100 mL round bottom flask. To the clear solution, the synthesized sodalite was added, and the resulting suspension was stirred at 100 °C for 24 h. The progress of the reaction was monitored through TLC. After completion of the reaction, sodalite was separated using a centrifuge, and the supernatant was collected. The supernatant was added to a separatory funnel containing DCM (10 mL), and the solution was washed with water (5 × 10 mL) to remove DMSO. Further, the separated organic layer was dried using sodium sulphate anhydrous and evaporated after filtration using a rotatory evaporator to give a crude product. The yields were obtained by comparing the ^{1}H NMR peaks (integrated) of the reactant with those of the product, as shown in section S2 of the ESI.†

3. Results and discussion

3.1 Characterization of fly ash

The freshly obtained fly ash (CFA) was passed through a sieve (63 μm) to obtain smaller-sized particles which constituted 69% of the material. These were then washed, gravity-separated (**S-CFA**), heated, and acid-treated to remove soluble impurities, volatile impurities, and metallic impurities and obtain **FA** which was used for further synthesis.

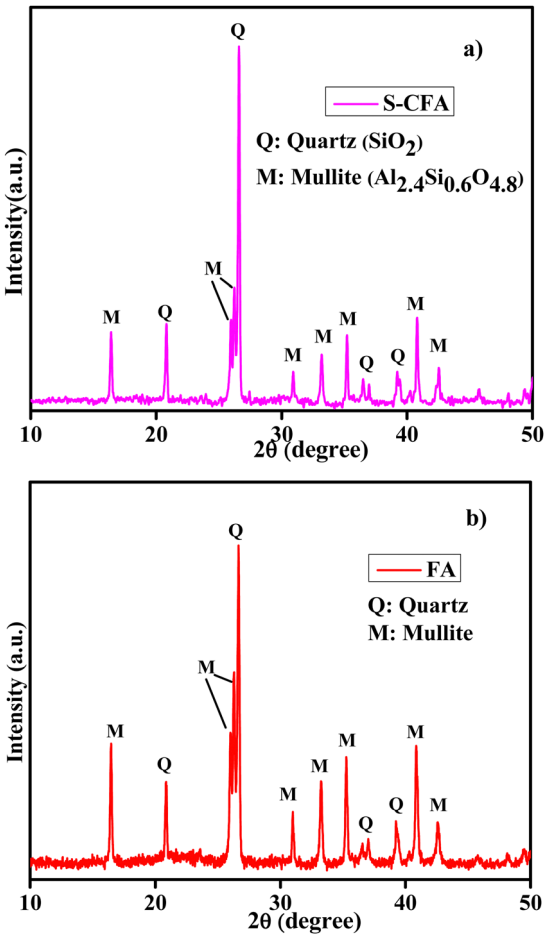

Fig. 2 The XRD patterns of (a) **S-CFA** and (b) **FA**.

S-CFA and **FA** were characterized using XRD, FE-SEM, and EDX. The XRD patterns in Fig. 2(a) show the presence of quartz (ICDD card no. 01-079-1906) and mullite (ICDD card no. 01-073-1389) in both samples. The quartz and mullite percentages were used to determine the Si : Al = 1.09 : 1 for **FA** (Fig. 2(b)). Fig. 3 shows the FE-SEM images of **S-CFA** and **FA** having spherical particles with an average particle size of 1.9 and 1.4 μm, respectively. The EDX analysis of **S-CFA** (Table 1) displayed the presence of Si and Al along with Ca, Mg, Ti, K, and Fe in trace amounts. EDX data of **FA** display the removal of Ca, Mg, and Ti, whereas the amounts of K and Fe were reduced significantly. The decreased values (rather than complete absence) upon acid treatment indicated the presence of K and Fe deep inside the **S-CFA** spheres which are still present in **FA**. The FTIR peaks at 1047 cm^{-1}, 790 cm^{-1}, 542 cm^{-1}, and 442 cm^{-1} for **FA**, as shown in Fig. 4(a), correspond to Si–O–Si, Si–O–Al, Al–O, and Si–O–Si (bending) bonds, respectively, and complimented the presence of silica and mullite.[35]

3.2 Characterization of the synthesized zeolite

The pretreated material **FA** was heat-treated with the desired amounts of NaOH and sodium aluminate. The fused material

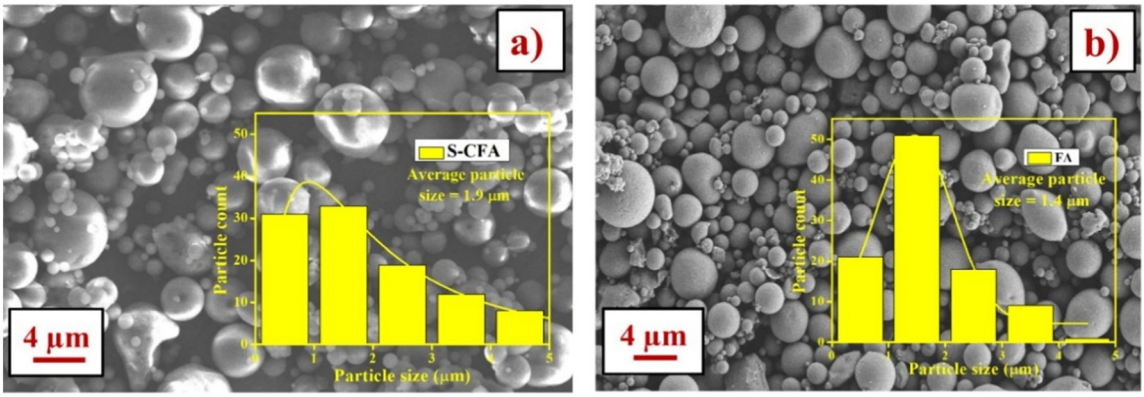

Fig. 3 FE-SEM images of (a) **S-CFA** and (b) **FA** having spherical particles and an average particle size (inset) of 1.9 and 1.4 μm, respectively.

Table 1 Comparison of the elemental composition of different materials used in this study from the EDS spectra

	Elements (atomic percentage)										
Samples	Ti	Al	Si	C	O	K	Ca	Mg	Fe	Na	F
S-FA	0.31	13.91	14.99	8.12	58.99	1.16	0.36	0.63	1.39	—	—
FA	—	15.10	15.99	9.79	57.48	0.64	—	—	0.99	—	—
Sodalite	—	10.54	10.60	12.77	55.36	—	—	—	0.58	10.16	—
Used-sodalite	—	8.91	9.31	19.22	54.28	—	—	—	0.66	6.48	1.14

was aged with an ultrasonic probe to obtain a gel solution that was conditioned using conventional heating, as described above, to crystallize into a zeolite (sodalite). The material was characterized using FTIR, XRD, and BET. Fig. 4(a) compares the FTIR spectra between the synthesized zeolite and **FA**. A significant shift in the peaks for Si–O–Si (949 cm^{-1} to 1047 cm^{-1}) and Si–O–Al (657 cm^{-1} to 790 cm^{-1}) bonds indicated morphological changes due to the rearrangement of Si and Al atoms. Also, the increased intensity of the above-mentioned peaks indicated the development of a more crystalline structure during the processing of **FA**.[17] Fig. 4(b) shows the XRD line profile data for the synthesized material depicting the absence of quartz and mullite phases. All the significant peaks matched the ICDD card number 01-076-1639, confirming the formation of sodalite.[27]

The FESEM images of the synthesized sodalite (Fig. 5(a) and (b)) displayed a clear difference in its morphology when compared with **FA** (Fig. 3(b)). It can be seen that the spherical morphology of **FA**, with an average size of 1.4 μm, transformed into porous spheres having an average size of 2.02 μm. The porosity of the synthesized material is attributed to the breaking of the initial spheres and the rearrangement of Si and Al atoms during the sodalite synthesis. The FTIR analysis also complements this observation. The EDX data of the sodalite (Table 1) show

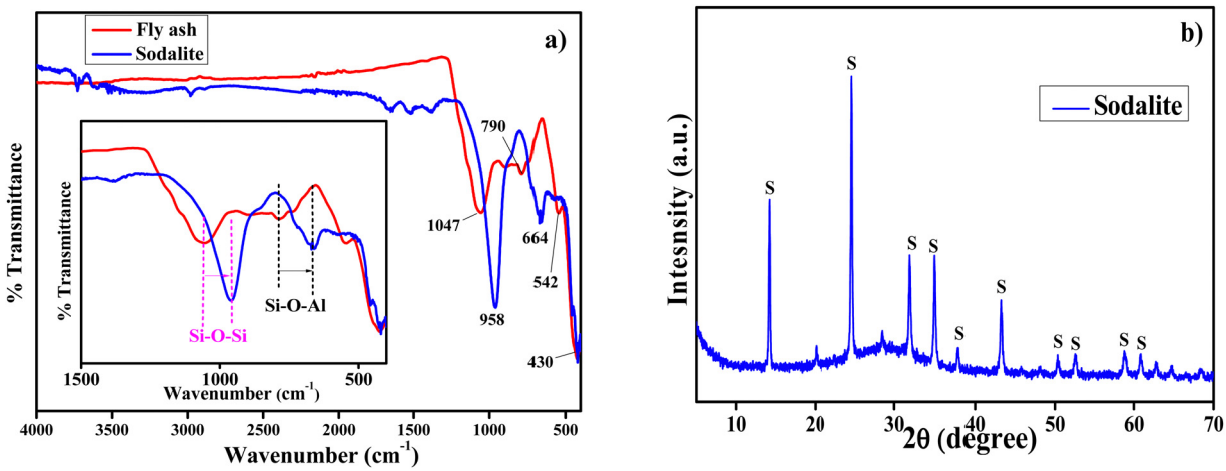

Fig. 4 (a) FTIR spectra of **FA** and sodalite showing an increased intensity and shift of the peaks indicating crystallinity of the sodalite and rearrangement of Si and Al atoms. (b) XRD pattern of sodalite showing the absence of the quartz and mullite phases.

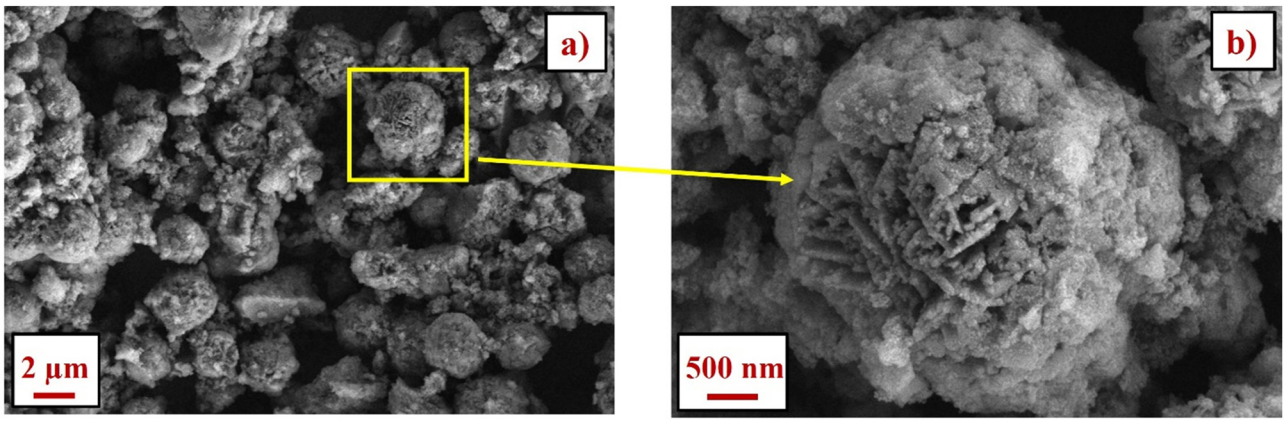

Fig. 5 FE-SEM images of (a) sodalite and (b) sodalite at high magnification.

approximately equal percentages for Si and Al and the presence of Na as a counterion in the framework.[36]

As discussed above, sodalite was envisaged as a substitute for the conventional base in diphenyl ether synthesis. Therefore, the point of zero charge (pH_{pzc}) was determined to ensure that there is no basicity in the proposed material due to any residual NaOH used during its synthesis. Fig. 6(a) shows that sodalite displayed a point of zero charge (pH_{pzc}) at pH 7.6, indicating a neutral behaviour and the absence of any residual basicity.[37] The BET analysis of sodalite using nitrogen adsorption–desorption exhibited a type-IV(a) isotherm (Fig. 6(b)), showing characteristics of a mesoporous material. The hysteresis loop exhibits an adsorption step between 0.014 and 1.00 and has a capillary condensation in the mesoporous region (>0.7) with a BET surface area of 22.13 $m^2\ g^{-1}$. Further, BJH analysis confirmed the mesoporous nature with an average pore size of 7 nm (Fig. 6(b)).[38]

Compared with the literature, the above analysis confirmed the transformation of CFA into sodalite. It was then used as a solid-state base to replace conventional ones for synthesizing diphenyl ethers.

3.3 Sodalite for diphenyl ether synthesis

The conventional synthesis of diphenyl ethers requires using bases like K_2CO_3, Cs_2CO_3, NaOH, and others to activate the nucleophile that attacks the electrophilic centre to generate an intermediate (Scheme 1).[39–41] The departure of the leaving group from the intermediate gives the desired product.

The literature shows that the surface hydroxy groups of the zeolites can be exploited under appropriate conditions to act as a base. Shanbhag *et al.* synthesized mesoporous zeolite with high aluminium content that acted as a solid base for industrially important organic reactions like Knoevenagel condensation, Claisen–Schmidt condensation, and acetylacetone cyclization.[42] Hiyoshi prepared nanocrystalline sodalite and used the synthesized material for epoxidation of α,β-unsaturated ketone using hydrogen peroxide.[43] As discussed above, sodalite, a solid-state base, has many advantages and was further explored for synthesizing diversely applied diphenyl ethers.

1-Fluoro-2-nitrobenzene and 2-methoxy phenol were used as substrates at 100 °C in the presence of 3 mole percent of the

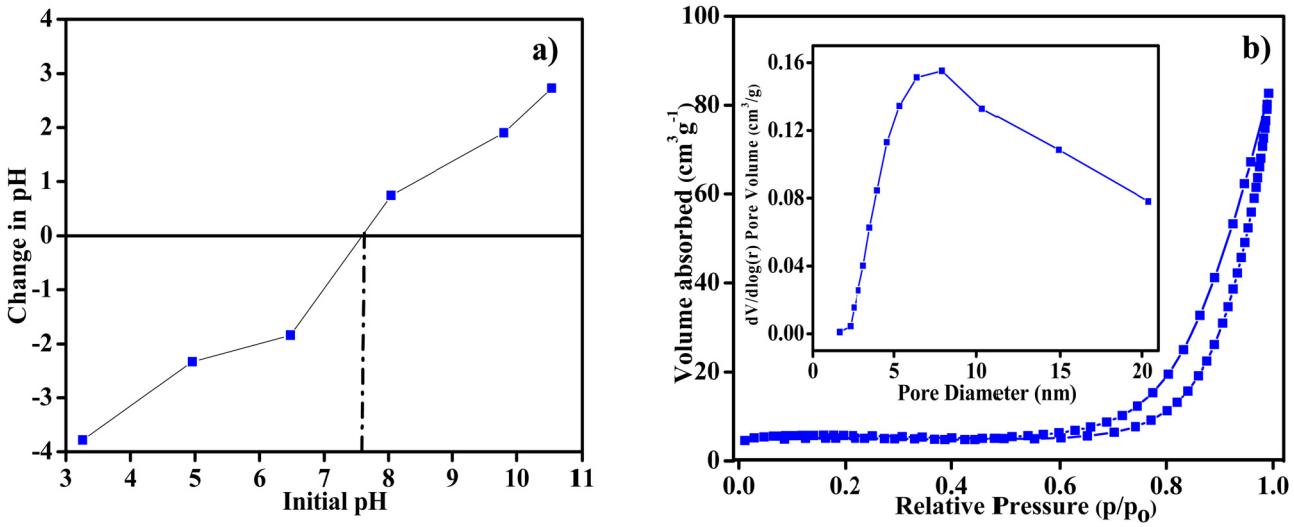

Fig. 6 (a) Point of zero charge determination and (b) N_2 adsorption–desorption isotherm for sodalite; the inset shows the pore size distribution.

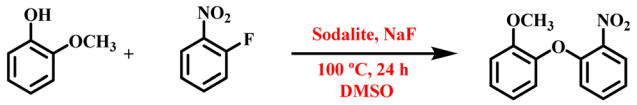

Scheme 2 Synthesis of diphenyl ether using sodalite and NaF.

sodalite to synthesize diphenyl ether (Scheme 2). Substantial product formation was observed only in the case of DMSO (20%) compared with toluene (1%) and DMF (8%). No product formation was observed in the case of acetonitrile, tetrahydrofuran, and methanol. A blank reaction without the sodalite in DMSO gave no product formation. The reaction time and temperature for the maximum yield were also optimized (Table S2, ESI†) to get the final parameters as 24 h and 100 °C.

The literature suggested using fluoride-based promoters to enhance the yield of organic reactions in the presence of zeolites as a base. Khalilzadeh *et al.* and others have used potassium fluoride as a promoter with clinoptilolite and alumina to synthesize diphenyl ethers.[34,44] The use of sodium fluoride as a promoter in this work also enhanced the yields. Further optimization was carried out (Table 2) using different mole per cent of sodalite and sodium fluoride (NaF). It can be seen that, compared to their sole presence, a high product yield required both sodalite and NaF in DMSO. Finally, one equivalent of phenol, 1-fluoro-2-nitrobenzene, NaF, and 10 mole percent of sodalite in aprotic DMSO were chosen as the final conditions for carrying out reactions with other substrates.

The scope of the above reaction was further explored with other nucleophiles (**2a–2n**) in the presence of 1-fluoro-2-nitrobenzene (**1**) as shown in Scheme 3 and Table 3.

Table 3 shows the yield of the synthesized diphenyl ethers ranging from 35 to 91% depending upon the substituents on

Table 2 Optimization of quantities for sodalite and NaF to get maximum yields

S. no.	Sodalite (mol%)	NaF (equivalent)	Percent yield[a]
1	NIL	1	11
2	6	NIL	22
3	10	NIL	35
4	12	NIL	40
5	6	1	61
6	10	1	72

[a] Based on NMR.

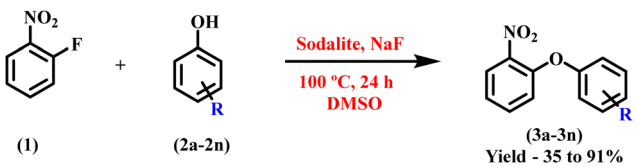

Scheme 3 General synthesis of different diphenyl ethers using one equivalent of 1-fluoro-2-nitrobenzene, phenols (**2a–2n**), NaF and 10 mole percent of sodalite in DMSO.

phenols. The substrates bearing methoxy, aldehyde (**2h** and **2j**), and nitro (**2l**) groups gave high yields ranging from 80 to 90%. It can be ascribed to the increased nucleophilicity of the phenol due to the interaction of respective functional group oxygens (NO_2, CHO, OCH_3) with the OH of the zeolite, as reported in the literature: Gorte *et al.* have theoretically shown the interaction of the aldehyde group with zeolite (Fig. 7(a)).[45] Nastase and Oluyinka *et al.* similarly evidenced the interaction of methoxy and nitro groups with zeolites, as shown in Fig. 7(b) and (c).[46,47] The low to moderate yields in the case of products **3i** (43%) and **3k** (64%) can be attributed to the steric hindrance and, in the case of **3e** (40%), **3f** (35%) and **3g** (49%) to the non-polar methyl substituent on the nucleophile. The *meta*-substituted methoxy (**2b**) and *ortho*, *para*-substituted chloro (**2m**) groups gave comparatively low conversion due to deactivation of the nucleophile.

The above results and reported theoretical studies direct that the nucleophilicity of the phenols in all substrates was enhanced due to their interaction with the –OH group on the surface of sodalite. Expected product formation was not observed for salicylic acid (**2d**) inspite of the phenolic proton presence. We believe that the presence of the –COOH group hindered –OH group interaction with sodalite by forming intermolecular hydrogen bonding (Fig. 7(d)).[48] This result confirms our conjecture regarding the importance of interaction of phenolic group with sodalite.[48]

Further, to explore the potential of this reaction with heterocyclic compounds, 8-hydroxyquinoline (**2n**) was reacted with 2-fluoro nitrobenzene using similar conditions. The product **3n** (78%) was purified and characterized as shown in section S4 of the ESI.† The good yields of **3n** suggest that optimized methodology can be explored further using sodalite for pharmaceutically important heterocyclic compounds.

3.4 Proposed reaction mechanism for synthesis of DPEs using sodalite

As discussed above, the synthesized sodalite's large pore diameter (7 nm) suggests that the interaction with organic substrates occurs at the surface rather than in pores. It is proposed that NaF activates the surface hydroxy groups (Scheme 4) to create a basic site. The created basic site abstracts the phenolic proton that further attacks the electrophilic centre of 1-fluoro-2-nitrobenzene, ultimately giving diphenyl ether by the departure of the leaving group.

3.5 Hot filtration test

A hot filtration test was carried out on product **3a** to understand the heterogeneous or homogeneous nature of sodalite (details in section S5 of the ESI†).[49] The reaction in the presence of sodalite gave a 58.5% yield after 8 h. Nearly the same yield of 59% after the hot filtration process (further heating the reaction mixture for 16 h) indicated that the synthesized sodalite works as a heterogeneous material.

Table 3 Scope of diphenyl ether synthesis using sodalite as a solid-state base

Entry	Phenol	Product	Percent yield[a]
1	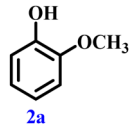 2a	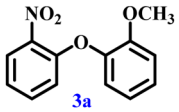 3a	72
2	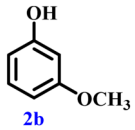 2b	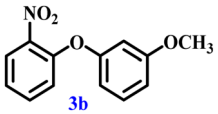 3b	41
3	 2c	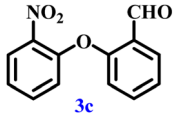 3c	83
4	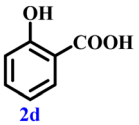 2d	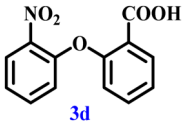 3d	No reaction
5	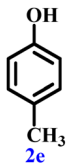 2e	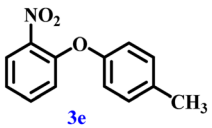 3e	40
6	 2f	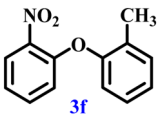 3f	35
7	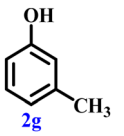 2g	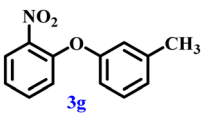 3g	49
8	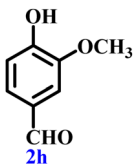 2h	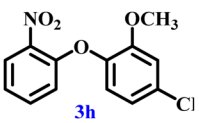 3h	80
9	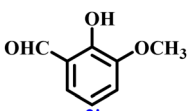 2i	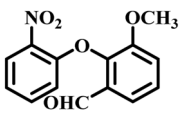 3i	43
10	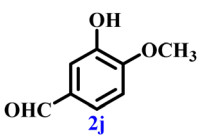 2j	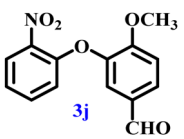 3j	91
11	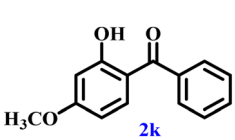 2k	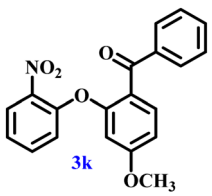 3k	64

Table 3 (*continued*)

Entry	Phenol	Product	Percent yield[a]
12	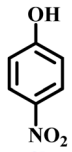 2l	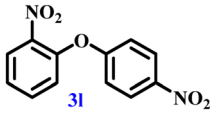 3l	90
13	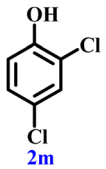 2m	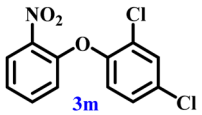 3m	64
14	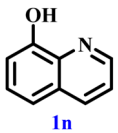 1n	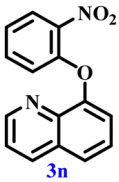 3n	78

[a] Based on NMR.

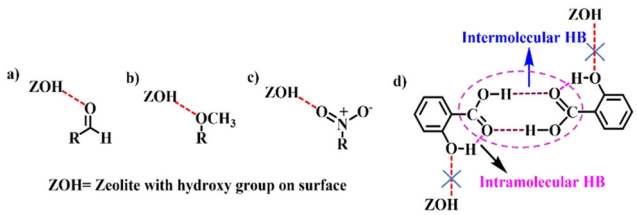

Fig. 7 The interaction of zeolite with the functional groups: (a) aldehyde, (b) methoxy and (c) nitro groups and (d) intermolecular and intramolecular interactions in salicylic acid.

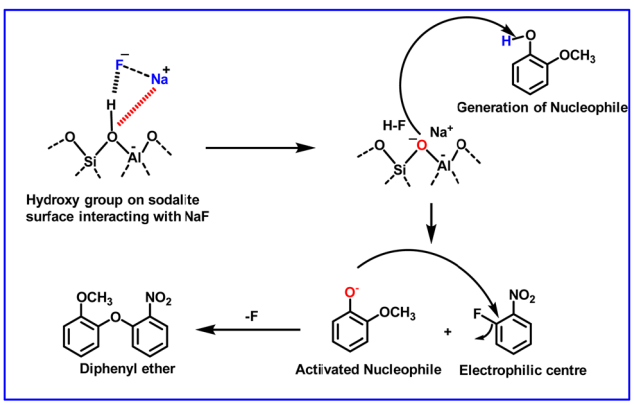

Scheme 4 Proposed mechanism for DPE synthesis using sodalite as a base activated by NaF.

3.6 Reusability attempts of sodalite

Attempts to reuse the sodalite did not yield encouraging results. The used sodalite was washed with water and ethanol

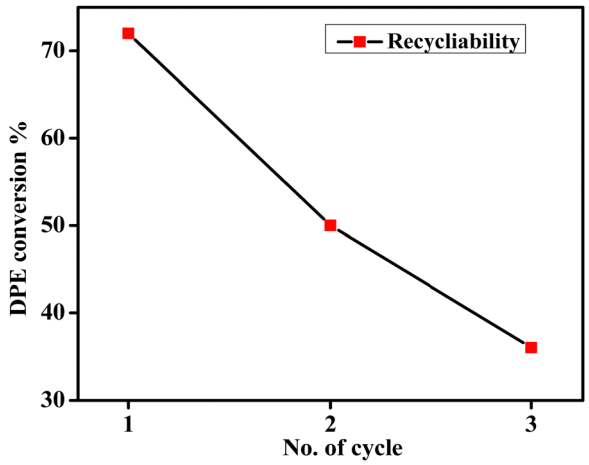

Fig. 8 Graph showing a considerable decrease in DPE conversion % after each cycle.

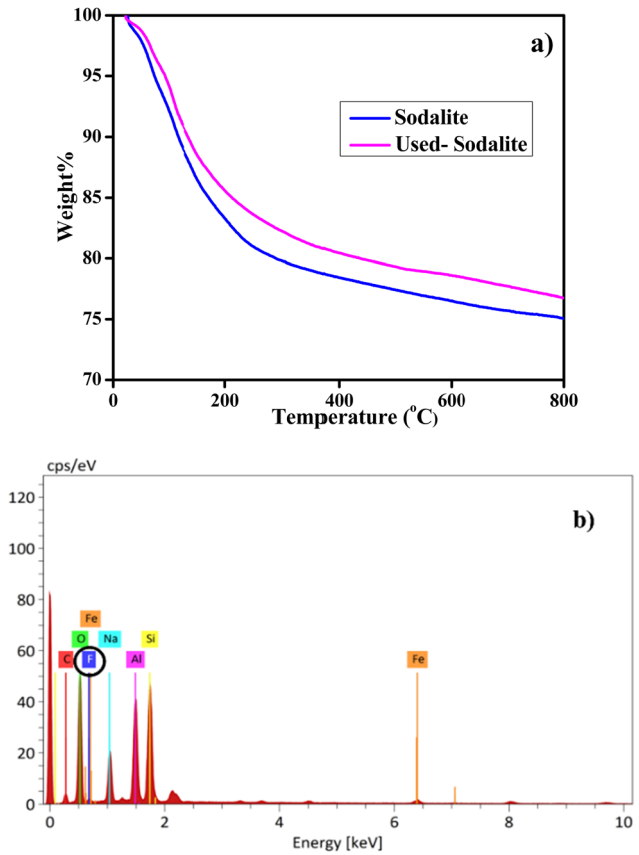

Fig. 9 (a) TGA data showing the comparison of sodalite and used-sodalite and (b) EDS spectra of used-sodalite.

(used-sodalite) and reused for DPE synthesis. Fig. 8 shows that the yield of DPE decreased to 50% (from 72%) after the second cycle and 30% after the next cycle.

Thermogravimetric analysis (TGA) was used to explore the cause of non-reusability. Fig. 9(a) displays the TGA data of sodalite and used-sodalite in the air atmosphere. In both samples, the weight loss follows the same pattern except that used-sodalite shows lower weight loss. The final weight loss at 750 °C in the case of sodalite was 3% more than that in the case of used-sodalite, implying the presence of certain extra materials in the sodalite. Further, the used-sodalite on EDX analysis displayed (Table 1) 1.14 atomic percent of fluorine. Unfortunately, as reported in the literature, attempts to remove fluorine gave no different results.[50]

3.7 Synthesis of sodalite and DPE: literature comparison

Table 4 compares the sodalite synthesis using different methods reported in the literature with this work. Here, an efficient aging methodology uses room temperature conditions and just 3 h to process **FA**, which upon simple oil bath heating gives crystallized sodalite.

Other than conventional bases, as discussed above, many groups have used solid-state bases for DPE synthesis. Table 5 shows the list of solid-state bases reported in the literature with the reported method. It can be seen that while other prevalent methods modified the commercially available zeolites and alumina with KF/copper, the present work merits the utilization of abundantly available coal fly ash to synthesize sodalite and its use in DPE synthesis without any further modification.

4. Conclusions

Overall, the work demonstrates a systematic methodology to convert coal fly ash into sodalite using ultrasonication and conventional heating. The prepared sodalite has been used as a solid-state base to synthesize diphenyl ethers to replace crown ethers and traditional bases like K_2CO_3 and Cs_2CO_3. It has been shown that several substituents can be accommodated in DPE synthesis with a moderate to excellent yield. The methodology was further extended to the heterocyclic compound by demonstrating the synthesis of compound **3n**. The present work opens the possibility of exploring other nucleophilic aromatic substitution reactions (SNAr) to replace conventional chemicals for a sustainable future.

Table 4 Synthesis of sodalite from coal fly ash using different methods

Material	Aging	Method	Conditions	Ref.
Hydroxy sodalite	70 °C, 1.5 h, stirring	Hydrothermal method	≥48 h at 140 °C	18
CTAB-sodalite	150 °C, 24 h in an air furnace	Calcination	550 °C for 3 h	4
Hydroxy sodalite	47 °C, 48 h, stirring	Hydrothermal method	140 °C, 48 h	38
Sodalite	6 days, rest	Crystallization	100 °C, 24 h	27
Sodalite	3 h, RT, ultrasonic probe	Conventional heating	110 °C, 16 h	**This work**

Table 5 Percentage yields of diphenyl ether using different zeolites and promoters

Material	Promotor	Percent yield of DPE	Ref.
Clinoptilolite (natural zeolite) impregnated with KF	KF	Up to 96	34
Copper(I)-exchanged zeolites (USY, MOR, β, and ZSM5)	Cu, Cs_2CO_3	Up to 89	29
Potassium fluoride-treated alumina	KF, 18-crown-6	Up to 99	44
Coal fly ash sodalite	NaF	Up to 91	**This work**

Author contributions

Aashima Mahajan: methodology, investigation, formal analysis, writing – original draft, preparation. Manmohan Chhibber: conceptualization, formal analysis, supervision, writing – review & editing. Loveleen K. Brar: conceptualization, formal analysis, supervision, writing – review & editing.

Data availability

No primary research results, software or code have been included and no new data were generated or analysed as part of this work.

Conflicts of interest

There are no conflicts of interest to declare.

Acknowledgements

MC and AM would like to thank TIET for the funds. The authors are grateful to SAI Labs, TIET, Patiala for providing the NMR facility; DST FIST Sponsored Material Characterization Facility, TIET, Patiala for XRD, FE-SEM, and EDS; DST FIST-sponsored Advanced Chemical Analysis Lab, TIET, Patiala for HRMS; CEEMS, TIET, Patiala for FTIR data; and the Department of Chemistry, IIT, Madras for BET results. The authors are thankful to the Department of Biotechnology, TIET, Patiala for permitting the use of the Ultrasonic Probe facility and Dr Bhupendrakumar Chudasama, Professor, DPMS, TIET, Patiala for TGA results.

References

1 A. Yousuf, S. O. Manzoor, M. Youssouf, Z. A. Malik and K. S. Khawaja, *J. Mater. Environ. Sci.*, 2020, **11**, 911–921.
2 A. R. K. Gollakota, V. Volli and C. M. Shu, *Sci. Total Environ.*, 2019, **672**, 951–989.
3 A. Ojha and P. Aggarwal, *Silicon*, 2022, **14**, 2453–2472.
4 K. M. Abas and N. A. Fathy, *Int. J. Environ. Sci. Technol.*, 2024, **21**, 5165–5184.
5 S. Gorai, *J. Mater. Environ. Sci.*, 2018, **9**, 385–393.
6 J. Gasparotto and K. D. B. Martinello, *Energy Geosci.*, 2021, **2**, 113–120.
7 M. K. Tiwari, S. Bajpai and U. K. Dewangan, *Int. Res. J. Eng. Technol.*, 2016, **3**, 949–956.
8 S. E. Kelechi, M. Adamu, O. A. U. Uche, I. P. Okokpujie, Y. E. Ibrahim and I. I. Obianyo, *Cogent Eng.*, 2022, **9**, 1–26.
9 X. Ren, L. Xiao, R. Qu, S. Liu, D. Ye, H. Song, W. Wu, C. Zheng, X. Wu and X. Gao, *RSC Adv.*, 2018, **8**, 42200–42209.
10 G. B. Balji, A. Surya, P. Govindaraj and G. M. Ponsakthi, *Inorg. Chem. Commun.*, 2022, **143**, 1–13.
11 O. B. Kotova, I. L. Shabalin, D. A. Shushkov and L. S. Kocheva, *Adv. Appl. Ceram.*, 2016, **115**, 152–157.
12 S. M. H. Asl, A. Ghadi, M. S. Baei, H. Javadian, M. Maghsudi and H. Kazemian, *Fuel*, 2018, **217**, 320–342.
13 B. T. Son, N. V. Long and N. T. N. Hang, *New J. Chem.*, 2021, **45**, 18552–18566.
14 A. Bhatt, S. Priyadarshini, A. A. Mohanakrishnan, A. Abri, M. Sattler and S. Techapaphawit, *Case Stud. Constr. Mater.*, 2019, **11**, 1–11.
15 M. Moshoeshoe, M. S. Nadiye-Tabbiruka and V. Obuseng, *Am. J. Mater. Sci.*, 2017, **7**, 196–221.
16 O. D. Ozdemir and S. Piskin, *Waste Biomass Valorization*, 2019, **10**, 143–154.
17 B. Makgabutlane, L. N. Nthunya, E. N. Nxumalo, N. M. Musyoka and S. D. Mhlanga, *ACS Omega*, 2020, **5**, 25000–25008.
18 J. M. Shabani, O. Babajide, O. Oyekola and L. Petrik, *Catalysts*, 2019, **9**, 1–14.
19 R. Deepika and M. G. Sethuraman, *Res. Chem. Intermed.*, 2022, **48**, 1111–1128.
20 Q. Sun, N. Wang and J. Yu, *Adv. Mater.*, 2021, **33**, 1–37.
21 W. Nabgan, A. A. Jalil, B. Nabgan, A. H. Jadhav, M. Ikram, A. Ul-Hamid, M. W. Ali and N. S. Hassan, *RSC Adv.*, 2022, **12**, 1604–1627.
22 Z. Wu, Z. He, Y. Xu, J. Wang, X. Lu, Q. Xia and D. Zhou, *J. Porous Mater.*, 2021, **28**, 1041–1048.
23 S. Narayanan, P. Tamizhdurai, V. L. Mangesh, C. Ragupathi, P. S. Krishnan and A. Ramesh, *RSC Adv.*, 2020, **11**, 250–267.
24 W. Sangthong and J. Sirijaraensre, *New J. Chem.*, 2023, **47**, 12191–12199.
25 M. Dyballa, K. Thorshaug, D. K. Pappas, E. Borfecchia, K. Kvande, S. Bordiga, G. Berlier, A. Lazzarini, U. Olsbye, P. Beato, S. Svelle and B. Arstad, *ChemCatChem*, 2019, **11**, 5022–5026.
26 H. Thakkar, A. Issa, A. A. Rownaghi and F. Rezaei, *Chem. Eng. Technol.*, 2017, **40**, 1999–2007.
27 M. C. Manique, L. V. Lacerda, A. K. Alves and C. P. Bergmann, *Fuel*, 2017, **190**, 268–273.
28 H. Valdés, R. F. Tardón and C. A. Zaror, *Chem. Eng. J.*, 2012, **211–212**, 388–395.
29 V. Magné, T. Garnier, M. Danel, P. Pale and S. Chassaing, *Org. Lett.*, 2015, **17**, 4494–4497.
30 A. D. Russell, *J. Antimicrob. Chemother.*, 2004, **53**, 693–695.
31 F. Rahman, K. H. Langford, M. D. Scrimshaw and J. N. Lester, *Sci. Total Environ.*, 2001, **275**, 1–17.

32 G. Yang, K. Yun, V. N. Nenkep, H. D. Choi, J. S. Kang and B. W. Son, *Chem. Biodivers.*, 2010, **7**, 2766–2770.
33 F. Li, Q. Wang, Z. Ding and F. Tao, *Org. Lett.*, 2003, **5**, 2169–2171.
34 M. A. Khalilzadeh, A. Hosseini and A. Pilevar, *Eur. J. Org. Chem.*, 2011, 1587–1592.
35 S. Sivalingam and S. Sen, *J. Environ. Manage.*, 2019, **235**, 145–151.
36 G. Ulian and G. Valdrè, *Minerals*, 2022, **12**, 1–15.
37 S. Mukherjee, S. Barman and G. Halder, *Groundw. Sustain. Dev.*, 2018, **7**, 39–47.
38 T. C. Aniokete, M. Ozonoh and M. O. Daramola, *Int. J. Renew. Energy Res.*, 2019, **9**, 1924–1937.
39 E. Lindstedt, R. Ghosh and B. Olofsson, *Org. Lett.*, 2013, **15**, 6070–6073.
40 M. Chhibber, G. Kumar, P. Parasuraman, T. N. C. Ramya, N. Surolia and A. Surolia, *Bioorg. Med. Chem.*, 2006, **14**, 8086–8098.
41 H. J. Chen, M. C. Tseng, I. J. Hsu, W. T. Chen, C. C. Han and S. G. Shyu, *Dalton Trans.*, 2015, **44**, 12086–12090.
42 G. V. Shanbhag, M. Choi, J. Kim and R. Ryoo, *J. Catal.*, 2009, **264**, 88–92.
43 N. Hiyoshi, *Appl. Catal., A*, 2012, **419–420**, 164–169.
44 J. S. Sawyer, E. A. Schmittling, J. A. Palkowitz and W. J. Smith, *J. Org. Chem.*, 1998, **63**, 6338–6343.
45 R. J. Gorte and D. White, *Top. Catal.*, 1997, **4**, 57–69.
46 S. A. F. Nastase, A. J. Logsdail and C. R. A. Catlow, *Phys. Chem. Chem. Phys.*, 2021, **23**, 17634–17644.
47 O. A. Oluyinka, A. V. Patel, B. A. Shah and M. I. Bagia, *Appl. Water Sci.*, 2020, **10**, 1–20.
48 S. Gholami, M. Aarabi and S. J. Grabowski, *J. Phys. Chem. A*, 2021, **125**, 1526–1539.
49 Y. S. Bao, L. Wang, M. Jia, A. Xu, B. Agula, M. Baiyin and B. Zhaorigetu, *Green Chem.*, 2016, **18**, 3808–3814.
50 Y. Gao, M. Li, Y. Ru and J. Fu, *Groundw. Sustain. Dev.*, 2021, **13**, 100567.

